Switching p-type to high-performance n-type organic electrochemical transistors via doped state engineering

Peiyun Li
Peking University
Junwei Shi
Peking University
Yuqiu Lei
Peking University
Zhen Huang
Peking University
Ting Lei (tinglei@pku.edu.cn)
Peking University https://orcid.org/0000-0001-8190-9483

Article

Keywords:

Posted Date: May 12th, 2022

DOI: https://doi.org/10.21203/rs.3.rs-1631706/v1

Version of Record: A version of this preprint was published at Nature Communications on October 10th, 2022. See the published version at https://doi.org/10.1038/s41467-022-33553-w.

Abstract

High-performance n-type organic electrochemical transistors (OECTs) are essential for constructing OECT-based logic circuits and enhancing the sensitivity of OECT-based sensors. However, the performances of n-type OECTs lag far behind that of the p-type ones due to the lack of effective molecular design strategies. Conventional wisdom posits that the LUMO energy level dictates the n-type performance. Herein, we show that engineering the doped state of conjugated polymers is more critical for n-type OECT polymers. By balancing more charges to the donor moiety, we could effectively switch a typical p-type polymer to high-performance n-type OECT materials. Based on this concept, the new polymer, P(gTDPP2FT), exhibits a record high n-type OECT performance with μC^* of 54.8 F cm^{-1} V^{-1} s^{-1}. The polymer also shows a record n-type OECT electron mobility of 0.35 cm^2 V^{-1} s^{-1}, leading to a fast response speed of τ_{on}/τ_{off} = 1.75/0.15 ms. DFT calculations and comparison studies show that the switching mechanism of the charge transport type is primarily due to the more uniformly distributed charges, stabilized negative polaron, and enhanced backbone planarity at negatively charged states. Unlike conventional molecular design strategies mainly focusing on lowering the lowest unoccupied molecular orbital (LUMO) level of the neutral polymers, our work highlights the critical role of understanding and engineering the polymer doped states.

Introduction

Organic electrochemical transistors (OECTs) have attracted increasing interest because they have shown broad applications in neural interfacing devices, biochemical sensors, and neuromorphic computing applications[1,2]. Various p-type polymers have been developed for high-performance OECTs with their figure of merit, μC^*, beyond 200 F cm^{-1} V^{-1} s^{-1}[3–5]. These p-type polymers also exhibit fast response speed with the τ_{on}/τ_{off} less than 1/0.1 ms, which are beneficial for real-time high-speed sensing applications[4]. To build complementary logic circuits for realizing high sensitivity and multiple device functions, n-type OECTs with comparable performance are necessary[6–8]. Unfortunately, compared to p-type ones, n-type OECT materials lag far behind in terms of both quantity and device performance, with μC^* usually less than 1 F cm^{-1} V^{-1} s^{-1} and τ_{on}/τ_{off} over 10 ms[9–16].

In the development of n-type organic field-effect transistor (OFET) materials, researchers usually introduce more electron-deficient moieties to lower the unoccupied molecular orbital (LUMO) energy level. This “lowering LUMO” strategy effectively enhances electron mobility and has promoted the fast development of n-type OFETs[16–24]. Inspired by this strategy, in the last three years, several strong electron-deficient n-type building blocks have been designed and used for OECTs, including naphthalene diimide (NDI)[9,11,25], benzodifurandione-based oligo(*p*-phenylene vinylene) (BDOPV)[26], bithiophene imide (BTI)[27,28], pyrazine-flanked diketopyrrolopyrrole (PzDPP)[11], 7,7'-diazaisoindigo (AIG)[29], and some ladder-type polymers[15,30]. The μC^* of the n-type OECT materials have been greatly enhanced from less than 0.1 F cm^{-1} V^{-1} s^{-1} to over 10 F cm^{-1} V^{-1} s^{-1}[9,28]. However, most of these works require the synthesis of complicated acceptor moieties with lengthy and expensive synthetic steps, which impedes the practical

applications of n-type OECTs. P-type materials, such as p(g2T2-g4T2) and gPBTTT, have not only simple molecular structures and short synthetic steps but also exhibit outstanding performances[5,31]. Such considerable disparity makes us wonder whether there is a simple but efficient approach to high-performance n-type OECT materials.

Unlike the interface doping characteristics in OFETs, the whole polymer films in OECTs are highly doped by electrolytes during operation[32,33]. We propose that the molecular properties at the neutral state cannot simply determine the charge carrier transport characteristics during OECTs operation; however, the electronic structures and properties at the doped state may play a decisive role. Here, we choose thiophene-flanked diketopyrrolopyrrole (TDPP), one of the most simple and commercially available building blocks for study. To date, all the OECT materials based on TDPP are p-type[34–36]. We found that the introduction of two fluorine atoms on thiophene donors makes p-type P(gTDPPT) switch to pure n-type P(gTDPP2FT) (Fig. 1). P(gTDPP2FT) exhibits a record high n-type OECT performance with μC^* of 54.8 F cm^{-1} V^{-1} s^{-1}. The polymer also shows record-high electron mobility of 0.35 cm^2 V^{-1} s^{-1} in water, with a fast response speed of τ_{on}/τ_{off} = 1.75/0.15 ms, which are among the shortest response times in n-type OECTs. Through theoretical and experimental exploration, we reveal that tuning the electronic properties at the polymer doped state result in enhanced backbone planarity, more uniform charge distributions, and better polaron stability, leading to higher n-type OECT performance.

Results And Discussions

Polymer synthesis and characterization. Commercially available TDPP (**1**) was used as the acceptor moiety. Compared with other n-type materials with long synthetic steps, the bromo-substituted TDPP (**3**) monomer used for polymerization only needs two steps to be obtained[11,15,25,36,37]. To compare the different electronic structures of the doped states, 2,5-bis(trimethylstannyl)thiophene (T) and 2,5-bis(trimethylstannyl)-3,4-difluorothiophene (2FT) were chosen to construct two similar polymers, namely P(gTDPPT) and P(gTDPP2FT) (Fig. 1). Ethylene glycol side chains (R) with farther branched positions were chosen for a closer π−π stacking distance and potentially enhanced charge carrier mobility, as we reported before[38,39]. Both polymers were obtained via Pd-catalyzed Stille coupling reactions in the presence of CuI as the co-catalyst[40]. Both polymers were purified by Soxhlet extraction and finally collected by chloroform. The molecular weights of the polymers were evaluated by gel permeation chromatography (GPC) using hexafluoroisopropanol (HFIP) as the eluent[4]. P(gTDPP2FT) shows a M_w/M_n = 65.04/30.70 kDa, comparable to other p- or n-type polymers[4]. Both polymers exhibit good thermal stability with high decomposition temperatures (Fig. S1, S2).

The optoelectronic properties of both polymers were evaluated using UV-Vis-NIR absorption spectra, cyclic voltammetry (CV), and spectroelectrochemistry (Fig. 2). The spectrum of P(gTDPP2FT) shows very similar maximum absorption peak (832 nm) and bandgap (1.34 eV) to that of P(gTDPPT) (836 nm, 1.36 eV) (Fig. 2a & b). Both spectra of P(gTDPPT) and P(gTDPP2FT) show a redshift in film and annealed film compared with the solution state, largely due to the further aggregation of the polymers. The 0-0/0-1

vibrational absorption peak ratio of P(gTDPP2FT) is larger than that of P(gTDPPT), suggesting a more planar backbone structure. The spectra results are consistent with the relaxed potential energy surface (PES) scan calculations. The PES scans at the dihedral angles of the TDPP-T/2FT show that both polymers have similar torsional barriers. P(gTDPP2FT) exhibits a dominant conformation at 0^o at the TDPP-2FT dihedral angle, while (P(gTDPPT) exhibits a 30^o dihedral angle (Fig. 2c).The measured ionic potentials (IP) and electron affinities (EA) of P(gTDPP2FT) are estimated to be 5.20 eV and 3.86 eV, higher than that of P(gTDPPT) (4.86 eV, 3.69 eV) (Fig. S3a & b), which is consistent with the DFT calculation results (Table S1, Fig. S4). Continuous CV sweep measurements of two polymers were explored in 0.1 M NaCl aqueous solution as the electrolyte, and both show good electrochemical stability (Fig. S3c & d). Interestingly, the DFT calculated torsion barriers of both polymers increase further after being n-doped. Besides, the bond length of TDPP-2FT (1.449 Å) is shorter than TDPP-T (1.454 Å), suggesting the enhanced conjugation of P(gTDPP2FT) (Fig. 2d).

Spectroelectrochemistry was performed to investigate the electrochemical characteristics of both polymers (Fig. 2e & f). Since P(gTDPPT) is a p-type OECT material, it was charged by oxidization, while P(gTDPP2FT) was charged by reduction. Driven by the positive voltage, chloride ions in the electrolyte penetrate into the P(gTDPPT) film to keep the charge neutrality of the polymer film. On the contrary, P(gTDPP2FT) was reduced by the negative voltage, and sodium ions are the counter ions. The electrochemical doping process generated polarons/bipolarons in both polymers films, showing new absorption bands in the long-wavelength region. The neutral polymers' absorption bands (700-900 nm) decrease, and the polaron/bipolaron absorption bands (900-1200 nm) rise.

OECT device fabrication and characterization. The OECT devices were fabricated using a photolithography and parylene patterning method[35]. The polymers were deposited using their chlorobenzene solution by spin-coating (see SI for more details). To evaluate the performance of an OECT material, the following equation based on the Bernards' model is often used (Eq. 1):[41]

$$g_m = (W/L) \bullet d \bullet \mu \bullet C^* \bullet |(V_{th} - V_{GS})| \qquad \text{(Eq. 1)}$$

where W, L, and d are the channel width, length, and film thickness, respectively, μ denotes the charge carrier mobility, C^* denotes the capacitance of the channel per unit volume, and V_{th} is the threshold voltage.

We applied both positive and negative gate voltages for both polymer devices. P(gTDPPT) shows typical p-type OECT behaviors, with a μC^* of up to 65.1 F cm^{-1} V^{-1} s^{-1}, while P(gTDPP2FT) shows an outstanding pure n-type OECT behaviors, with a high μC^* of up to 54.8 F cm^{-1} V^{-1} s^{-1} (Fig. 3a-d, Table 1), which is a record value in the literature reported to date. Both polymers show a similar threshold voltage with an absolute value of around 0.6 V. To exclude the potential side-chain effects, we also synthesized P(lgTDPP2FT), with the same backbone as P(gTDPP2FT) but a linear side chain (Fig. S5). P(lgTDPP2FT) also shows n-type OECT behaviors with a high μC^* of 20.4±1.0 F cm^{-1} V^{-1} s^{-1}, which demonstrates the high n-type OECT performance of P(gTDPP2FT) come from the introduction of F atoms, not the side

chains. The volumetric capacitance (C^*) was measured by electrochemical impedance spectrum (EIS) (Fig. S6). The maximal C^* was extracted with an average value of 161 F cm^{-3} for P(gTDPPT), and 156 F cm^{-3} for P(gTDPP2FT). Based on the μC^* and C^* values, the hole/electron mobility (μ) was calculated to be 0.40 $cm^2 V^{-1} s^{-1}$ for P(gTDPPT) and 0.35 $cm^2 V^{-1} s^{-1}$ for P(gTDPP2FT). Furthermore, we tested the transient characteristics of their OECT devices to evaluate the response speed of both polymers (Fig. 3e & f). A pulse was applied to the gate electrode, and a DC voltage with an absolute value of 0.6 V was applied to the drain electrode. The response time was estimated by an exponential fitting of the I_{DS}. P(gTDPPT) and P(gDPP2FT) both exhibit short response times, with τ_{on}/τ_{off} of 0.46/0.08 ms and 1.75/0.15 ms, respectively. The high μ and fast response characteristics make P(gTDPP2FT) a promising material for real-time high-speed sensing applications. The two polymers were used to fabricate complementary inverters because of their matched operating voltage and device performance. When the supply voltage (V_{DD}) is set to 0.8 V and the input voltage (V_{In}) is swept from 0 to 0.8 V, a relatively high gain value ($\partial V_{Out}/\partial V_{In}$) of 26.8 was obtained (Fig. 3g). The μC^* and μ of P(gTDPP2FT) are both record values, and the response times are among the shortest in n-type OECT materials (Fig. 3h & i)[25,27-30,38,42].

Table 1. Summary of the OECTs Performance and Molecular Packing Parameters of the Polymers.

	Type	g_m[a] (mS)	d (nm)	V_{th}[b] (V)	I_{on}/I_{off}	μC^*[c] (F/cm V s)	μ[d] (cm^2/V s)	C^* (F cm^{-3})	τ_{on} (ms)	τ_{off} (ms)	$d_{lamellar}$ (Å)	$d_{\pi-\pi}$ (Å)
P(gTDPPT)	p	1.18	60.5	-0.60	5×10^6	65.1 (45.9±13.7)	0.40	161	0.46	0.08	26.18	3.68
P(gTDPP2FT)	n	0.93	60.6	0.62	5×10^6	54.8 (42.2±6.5)	0.35	156	1.75	0.15	27.32	3.68

[a]The W/L of all the devices is 100/10 μm. All the OECT devices were operated in a 0.1 M NaCl aqueous solution. [b]V_{th} was determined by extrapolating the corresponding $I_{DS}^{1/2}$ vs. V_{GS} plots. [c]Four devices were tested and computed for each polymer. μC^* was calculated according to Eq. 1. [d]μ was calculated from the μC^* and the measured volumetric capacitance C^*.

Film microstructure characterization. Grazing incidence wide-angle X-ray scattering (GIWAXS) and atomic force microscope (AFM) were employed to explore the molecular packing and morphology. Both P(gTDPPT) and P(gTDPP2FT) show typical face-on molecular packings (Fig. 4a & b). The two polymers have the same π-π stacking distance of 3.68 Å, and P(gTDPP2FT) shows a slightly larger lamellar distance (Table 1 and Fig. S7). P(gTDPP2FT) exhibits three in-plane lamellar scattering peaks with narrower half peak width, (100), (200), and (300), suggesting its more ordered molecular packing and higher crystallinity. Both polymer films are smooth with small root-mean-square (RMS) roughness in atomic force microscope (AFM) height images (Fig. 4c & d). P(gTDPP2FT) film shows fiber-like textures, while P(gTDPPT) film is more amorphous. The AFM results are consistent with GIWAXS results.

Understanding of the "doped state engineering" strategy. The outstanding OECTs performances of P(gTDPP2FT) are out of our expectations because its LUMO energy level is rather high compared with several typical n-type OECT materials (Fig. 5a). P(gPyDPPT) was also synthesized for comparison (Fig. 5b). P(gPyDPP-T2) with bithiophene as the donor moiety was reported by Giovannitti *et al.* It showed very poor p-type OECT performance[34]. We synthesized P(gPyDPPT) here, and it shows poor n-type OECT performance with μC^* of 0.07 F cm^{-1} V^{-1} s^{-1} (Fig. S8). The introduction of pyridine and F atoms both reduce the LUMO energy level of P(gTDPPT) and the difference value between the LUMO energy level of P(gPyDPPT) and P(gPyDPP2FT) is less than 0.1 eV (Fig. 5c). We summarized the relationship between LUMO energy level and device performance of several n-type OECT polymers (Fig. 5a). The μC^* value is not correlated well with LUMO energy levels. These results indicate that high-performance n-type OECT materials cannot be simply obtained by lowering the LUMO energy levels.

OECT materials usually work under highly doped states. We propose that the molecular properties under highly doped states might significantly affect the charge transport properties. Therefore, we calculated the properties of the three polymers' doped states. The energy difference between the neutral and negatively charged state ($\Delta E = E_{negative} - E_{neutral}$) of P(gPyDPPT) is −48.93 kcal/mol, which is much smaller than that of P(gTDPP2FT) (−52.99 kcal/mol), and even smaller than that of P(gTDPPT) (−49.01 kcal/mol). These results suggest that the negative polarons on P(gTDPP2FT) backbone are more stable, and the stability is not related to the polymer LUMO energy levels (Fig. 5a, Fig. S9). We also calculated the charge distribution of the three polymers relative to their neutral state (Fig. 5d-f, Fig. S10). The negative charges of n-doped [P(gTDPP2FT)]$^{1-}$ distribute on the whole polymer chain, whereas the negative charges of [P(gPyDPPT)]$^{1-}$ are mostly localized in the center of the chain. Compared to [P(gTDPPT)]$^{1-}$, the negative charges of [P(gTDPP2FT)]$^{1-}$ on the T moieties next to DPP are shared by the donor moiety 2FT (black and red arrows in Fig. 5d & f), which makes the charge distribution more balanced. On the contrary, the positive charges of P(gTDPPT) are the most delocalized, while the positive charges of the other two polymers are located on one end of the chain. Besides, the distribution of dihedral angles between fragments is quite different for the three polymers (Fig. 5g-i). P(gTDPP2FT) shows the smallest dihedral angles along the polymer backbone at the neutral state, which decrease further after being negatively charged. Relatively large dihedral angles of P(gTDPPT) decrease a little after being negatively charged. Conversely, P(gPyDPPT) exhibits the largest dihedral angles, which do not change much after being both positively and negatively charged. All these charge and dihedral angle distributions prove that the introduction of fluorine atoms in P(gTDPP2FT) not only lowers the LUMO energy level but also enhances the polymer backbone planarity, delocalizes, and stabilizes the negative polaron. These favorable factors might explain the n-type charge transport behavior and high electron mobility of P(gTDPP2FT) under strong electrochemical n-doping.

Conclusion

In conclusion, we have proposed a "doped state engineering" strategy to design n-type OECT polymers and effectively switch a typical p-type OECT polymer to a high-performance n-type OECT polymer. We

demonstrate that the switching mechanism of the charge transport type is primarily due to the enhanced backbone planarity, more uniform negative charge distribution, and more stable negative polaron at n-doped states. These features make polymer P(gTDPP2FT) exhibit pure n-type charge transport behaviors with record-high electron mobility of 0.35 $cm^2 V^{-1} s^{-1}$ in water, record-high μC^* values of 54.8 F $cm^{-1} V^{-1} s^{-1}$, and a fast response speed of τ_{on}/τ_{off} = 1.75/0.15 ms. Our work reveals the significant differences in the electronic properties between the charged and neutral states and highlights a new “doped state engineering” strategy for future high-performance OECT materials design.

References

1. Rivnay J, *et al.* Organic electrochemical transistors. Nat. Rev. Mater. **3**, 17086 (2018).
2. Zeglio E, Inganas O. Active materials for organic electrochemical transistors. Adv. Mater. **30**, e1800941 (2018).
3. Moser M, *et al.* Polaron delocalization in donor-acceptor polymers and its impact on organic electrochemical transistor performance. Angew. Chem. Int. Ed. **60**, 7777–7785 (2020).
4. Jia H, *et al.* Engineering donor–acceptor conjugated polymers for high-performance and fast-response organic electrochemical transistors. J. Mater. Chem. C **9**, 4927–4934 (2021).
5. Hallani RK, *et al.* Regiochemistry-driven organic electrochemical transistor performance enhancement in ethylene glycol-functionalized polythiophenes. J. Am. Chem. Soc. **143**, 11007–11018 (2021).
6. Romele P, *et al.* Multiscale real time and high sensitivity ion detection with complementary organic electrochemical transistors amplifier. Nat. Commun. **11**, 3743 (2020).
7. Yang CY, *et al.* A high-conductivity n-type polymeric ink for printed electronics. Nat. Commun. **12**, 2354 (2021).
8. Griggs S, Marks A, Bristow H, McCulloch I. N-type organic semiconducting polymers: Stability limitations, design considerations and applications. J. Mater. Chem. C **9**, 8099–8128 (2021).
9. Giovannitti A, *et al.* N-type organic electrochemical transistors with stability in water. Nat. Commun. **7**, 13066 (2016).
10. Sun H, *et al.* Complementary logic circuits based on high-performance n-type organic electrochemical transistors. Adv. Mater. **30**, 1704916 (2018).
11. Giovannitti A, *et al.* The role of the side chain on the performance of n-type conjugated polymers in aqueous electrolytes. Chem. Mater. **30**, 2945–2953 (2018).
12. Paterson AF, *et al.* On the role of contact resistance and electrode modification in organic electrochemical transistors. Adv. Mater. **31**, e1902291 (2019).
13. Savva A, *et al.* Solvent engineering for high-performance n-type organic electrochemical transistors. Adv. Electron. Mater. **5**, 1900249 (2019).
14. Paterson AF, *et al.* Water stable molecular n-doping produces organic electrochemical transistors with high transconductance and record stability. Nat. Commun. **11**, 3004 (2020).

15. Chen X, *et al.* N-type rigid semiconducting polymers bearing oligo(ethylene glycol) side chains for high-performance organic electrochemical transistors. Angew. Chem. Int. Ed. **60**, 9368–9373 (2021).
16. Cong S, *et al.* Donor functionalization tuning the n-type performance of donor–acceptor copolymers for aqueous-based electrochemical devices. Adv. Funct. Mater., 10.1002/adfm.202201821 (2022).
17. Lei T, *et al.* Ambipolar polymer field-effect transistors based on fluorinated isoindigo: High performance and improved ambient stability. J. Am. Chem. Soc. **134**, 20025–20028 (2012).
18. Lei T, *et al.* A bdopv-based donor-acceptor polymer for high-performance n-type and oxygen-doped ambipolar field-effect transistors. Adv. Mater. **25**, 6589–6593 (2013).
19. Sun B, *et al.* Record high electron mobility of 6.3 cm(2) v(-)(1) s(-)(1) achieved for polymer semiconductors using a new building block. Adv. Mater. **26**, 2636–2642 (2014).
20. Feng K, Guo H, Sun H, Guo X. N-type organic and polymeric semiconductors based on bithiophene imide derivatives. Acc. Chem. Res. **54**, 3804–3817 (2021).
21. Yang J, *et al.* Insight into high-performance conjugated polymers for organic field-effect transistors. Chem **4**, 2748–2785 (2018).
22. Lei T, Wang JY, Pei J. Design, synthesis, and structure-property relationships of isoindigo-based conjugated polymers. Acc. Chem. Res. **47**, 1117–1126 (2014).
23. Gao Y, *et al.* Multifluorination toward high-mobility ambipolar and unipolar n-type donor-acceptor conjugated polymers based on isoindigo. Adv. Mater. **29**, 1606217 (2017).
24. Yao J, *et al.* Significant improvement of semiconducting performance of the diketopyrrolopyrrole-quaterthiophene conjugated polymer through side-chain engineering via hydrogen-bonding. J. Am. Chem. Soc. **138**, 173–185 (2016).
25. Ohayon D, *et al.* Influence of side chains on the n-type organic electrochemical transistor performance. ACS Appl. Mater. Interfaces **13**, 4253–4266 (2021).
26. Wang YZ, *et al.* Green synthesis of lactone-based conjugated polymers for n-type organic electrochemical transistors. Adv. Funct. Mater. **32**, 2111439 (2022).
27. Feng K, *et al.* Fused bithiophene imide dimer-based n-type polymers for high-performance organic electrochemical transistors. Angew. Chem. Int. Ed. **60**, 24198–24205 (2021).
28. Feng K, *et al.* Cyano-functionalized n-type polymer with high electron mobility for high-performance organic electrochemical transistors. Adv. Mater., 10.1002/adma.202201340, e2201340 (2022).
29. Parr ZS, *et al.* From p- to n-type mixed conduction in isoindigo-based polymers through molecular design. Adv. Mater., 10.1002/adma.202107829, e2107829 (2022).
30. Marks A, *et al.* Synthetic nuances to maximize n-type organic electrochemical transistor and thermoelectric performance in fused lactam polymers. J. Am. Chem. Soc. **144**, 4642–4656 (2022).
31. Moser M, *et al.* Side chain redistribution as a strategy to boost organic electrochemical transistor performance and stability. Adv. Mater. **32**, e2002748 (2020).
32. Matta M, *et al.* Ion coordination and chelation in a glycolated polymer semiconductor: Molecular dynamics and x-ray fluorescence study. Chem. Mater. **32**, 7301–7308 (2020).

33. Dong BX, *et al.* Influence of side-chain chemistry on structure and ionic conduction characteristics of polythiophene derivatives: A computational and experimental study. Chem. Mater. **31**, 1418–1429 (2019).
34. Giovannitti A, *et al.* Energetic control of redox-active polymers toward safe organic bioelectronic materials. Adv. Mater. **32**, e1908047 (2020).
35. Luo X, *et al.* Designing donor–acceptor copolymers for stable and high-performance organic electrochemical transistors. ACS Macro Lett. **10**, 1061–1067 (2021).
36. Samuel JJ, *et al.* Single-component cmos-like logic using diketopyrrolopyrrole-based ambipolar organic electrochemical transistors. Adv. Funct. Mater. **31**, 2102903 (2021).
37. Maria IP, *et al.* The effect of alkyl spacers on the mixed ionic-electronic conduction properties of n-type polymers. Adv. Funct. Mater. **31**, 2008718 (2021).
38. Shi JW, *et al.* Revealing the role of polaron distribution on the performance of n-type organic electrochemical transistors. Chem. Mater. **34**, 864–872 (2022).
39. Lei T, Dou JH, Pei J. Influence of alkyl chain branching positions on the hole mobilities of polymer thin-film transistors. Adv. Mater. **24**, 6457–6461 (2012).
40. Carsten B, *et al.* Stille polycondensation for synthesis of functional materials. Chem. Rev. **111**, 1493–1528 (2011).
41. Bernards DA, Malliaras GG. Steady-state and transient behavior of organic electrochemical transistors. Adv. Funct. Mater. **17**, 3538–3544 (2007).
42. Wu HY, *et al.* Influence of molecular weight on the organic electrochemical transistor performance of ladder-type conjugated polymers. Adv. Mater. **34**, e2106235 (2022).

Declarations

Acknowledgements

This work is supported by the National Natural Science Foundation of China (22075001 and 92156019) and the Open Fund of the State Key Laboratory of Luminescent Materials and Devices, South China University of Technology (2021-skllmd-02). The computational part is supported by High-Performance Computing Platform of Peking University.

Author contributions

P.L. and J.S. contributed equally to this work. J.S. and Z.H. synthesized the polymer and performed some characterization. P.L. and Y.L. performed device fabrication and characterization. P.L. performed DFT calculations. P.L., J.S., and T.L. wrote the manuscript. All the authors revised and approved the manuscript.

Competing interests

The authors declare no competing financial or non-financial interests.

Additional information

Supplementary information is available in the online version of the paper.

Figures

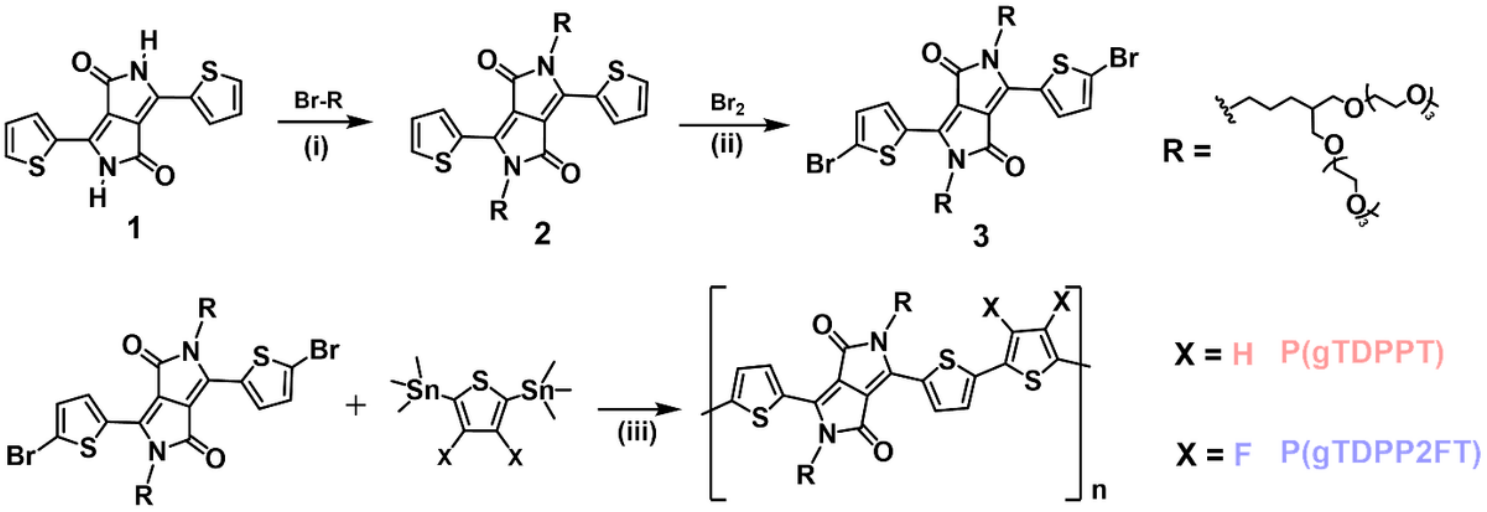

Figure 1

Synthetic Routes to the Polymers, P(gTDPPT) and P(gTDPP2FT). Reagents and conditions: ( ) K_2CO_3, DMF, 110 ^oC, 12 h; ( ) Br_2, DCM, 0 ^oC, 2 h; ( ) $Pd(PPh_3)_4$, CuI, Toluene/NMP (v/v = 1/1), 110 ^oC, 48 h.

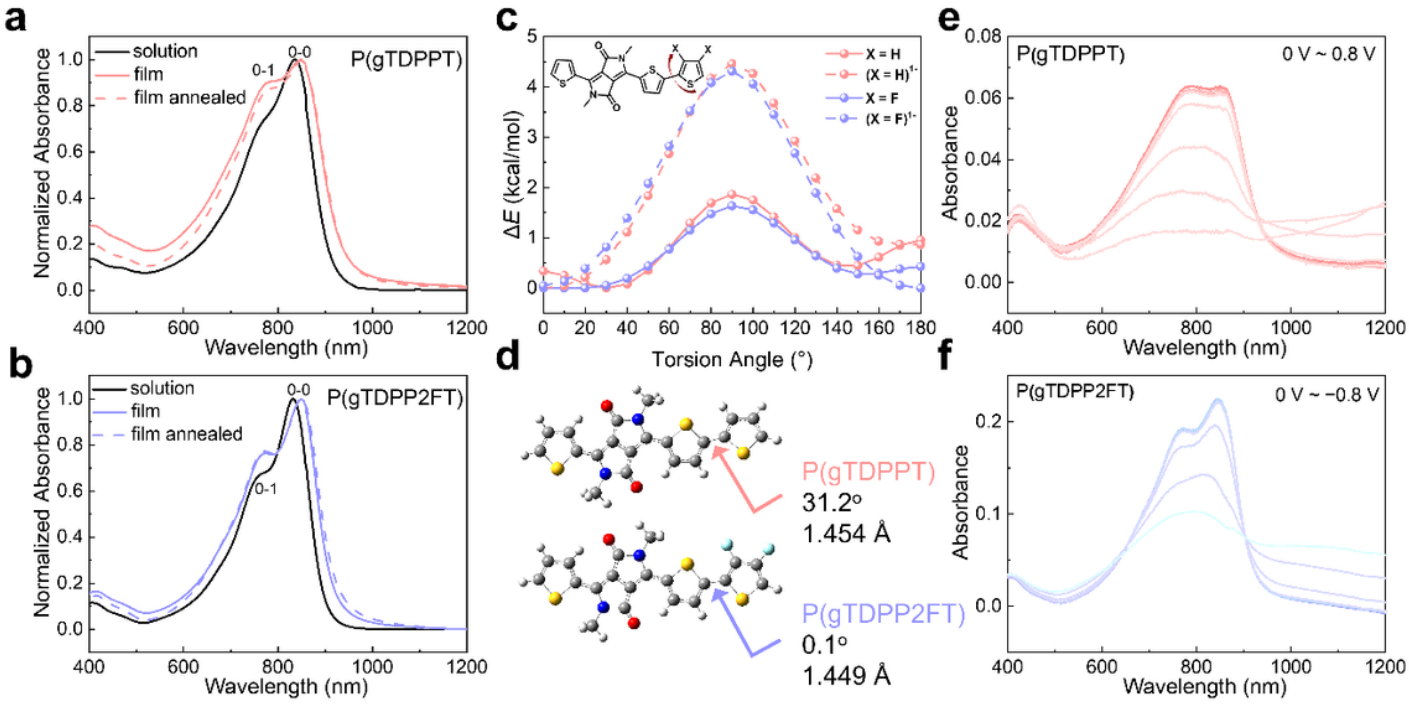

Figure 2

Optoelectronic properties of both polymers. Normalized UV-vis-NIR absorption spectra of **a** P(gTDPPT) and **b** P(TDPP2FT) in solution, in thin film, and in annealed film (80 °C, 10 min). **c** Comparison of the relaxed PES scans of the dihedral angles for the monomers of P(gTDPPT) and P(gTDPP2FT) in the neutral and negatively charged states. **d** Optimized backbone structures, the bond lengths, and dihedral angles for the monomers. Electrochemical absorption spectra of **e** P(gTDPPT) and **f** P(TDPP2FT) in 0.1 M NaCl aqueous solution.

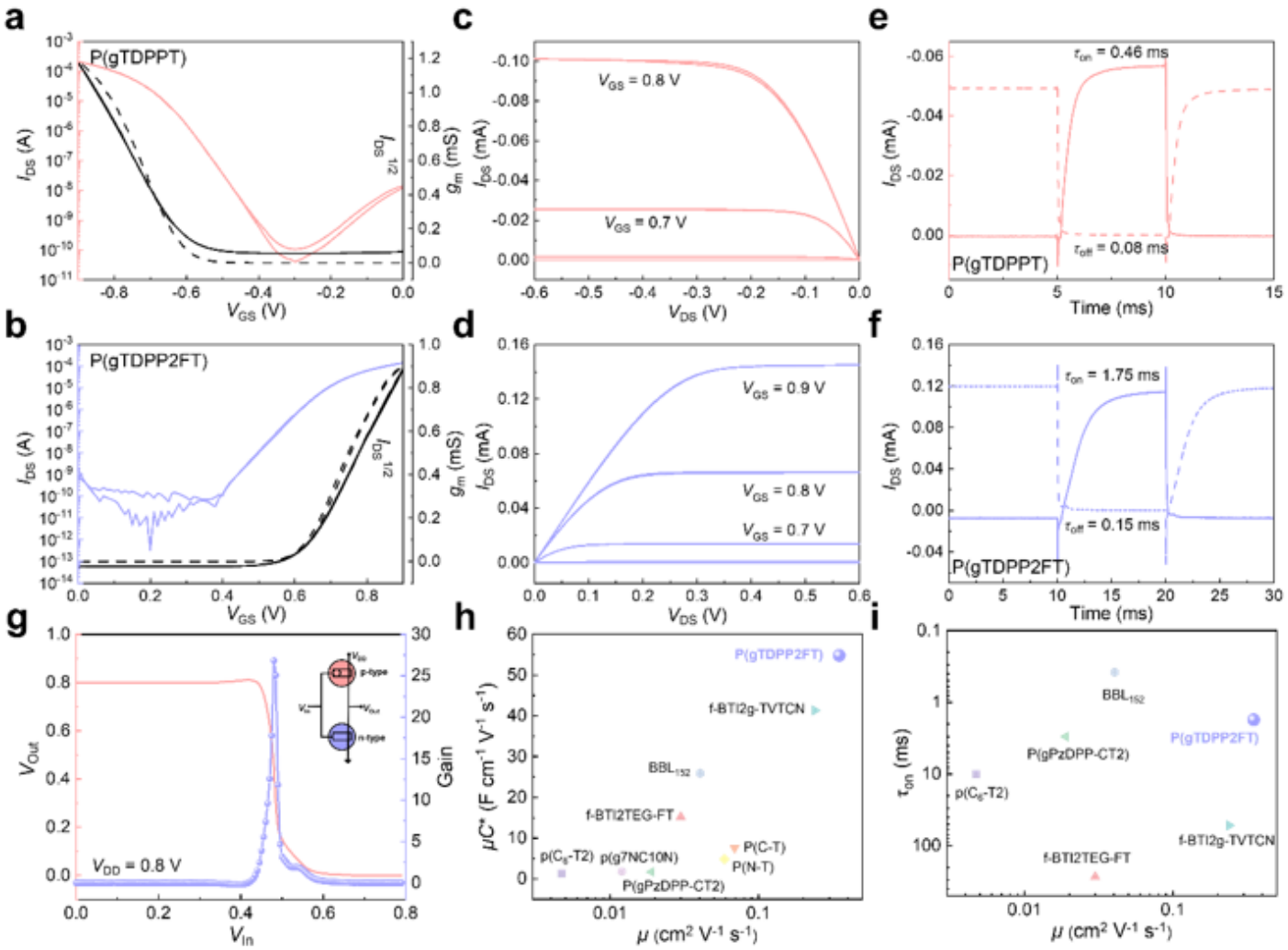

Figure 3

OECT device characterization of P(gTDPPT) and P(gTDPP2FT). a & **b** Transfer characteristics, and **c** & **d** output characteristics of P(gTDPPT) and P(gTDPP2FT). The dash lines are the curve of g_m. **e** & **f** Transient on/off curves with V_{GS} of 0~−0.9 and 0~0.9 V for P(gTDPPT) and P(gTDPP2FT), respectively. Device configuration: W/L = 100/10 μm, $|V_{DS}|$= 0.6 V. **g** Voltage transfer characteristics and gain of the complementary inverter based on P(gTDPPT) and P(gTDPP2FT). Insert is the circuit diagram of the complementary inverter. Device configuration: W/L = 100/10 μm. Comparison of the **h** μC^* and μ, and **i** τ_{on} and μ values of P(gTDPP2FT) with other reported n-type OECT materials[25,27-30,38,42].

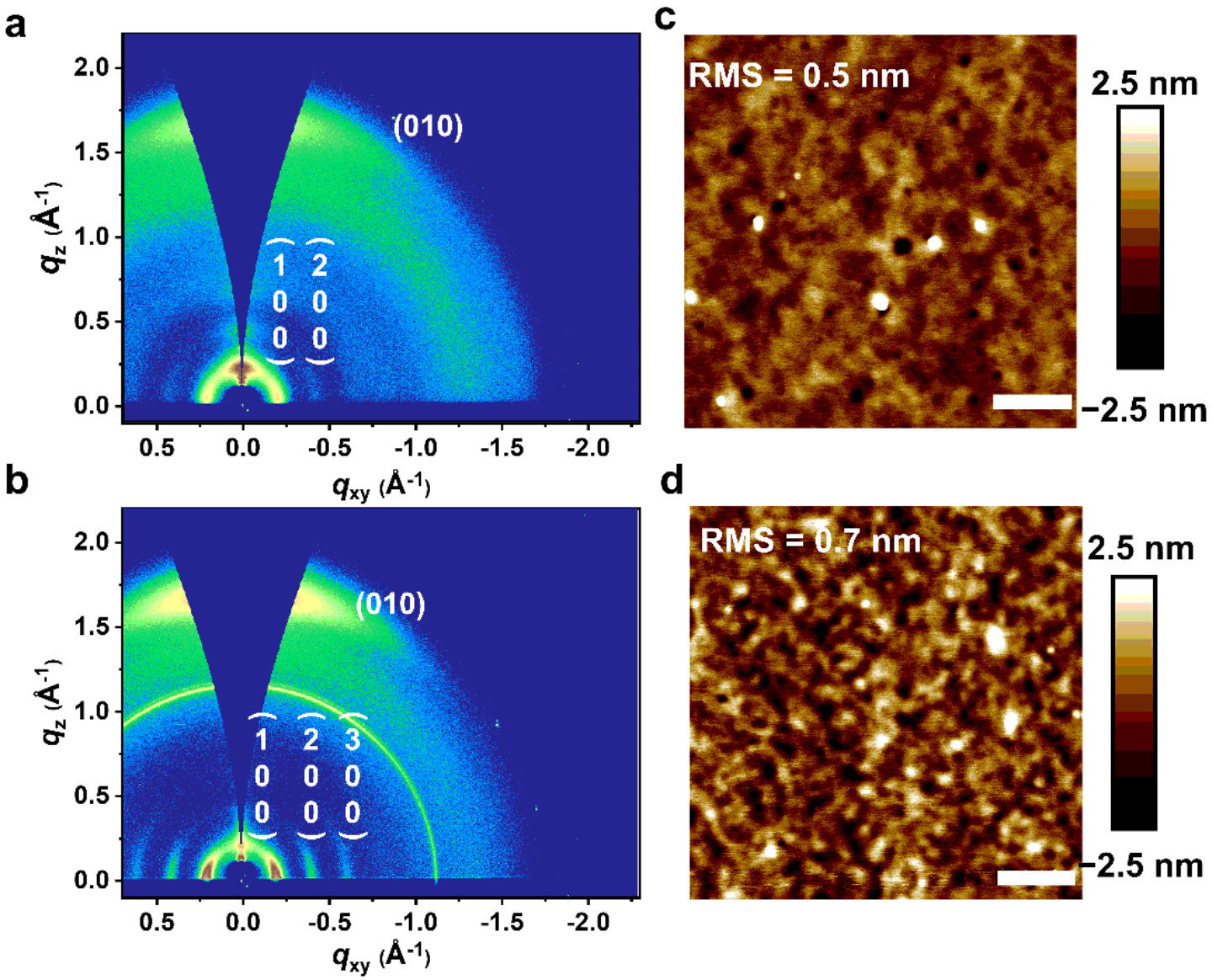

Figure 4

Molecular packing and morphology characterization. a & **b** 2D-GIWAXS patterns of P(gTDPPT) and P(gTDPP2FT). The diffraction signal around 1.23 Å^{-1} in Fig. 3b is from the silicon substrate. **c** & **d** AFM height images of P(gTDPPT) and P(gTDPP2FT) films. The scale bars are 400 nm.

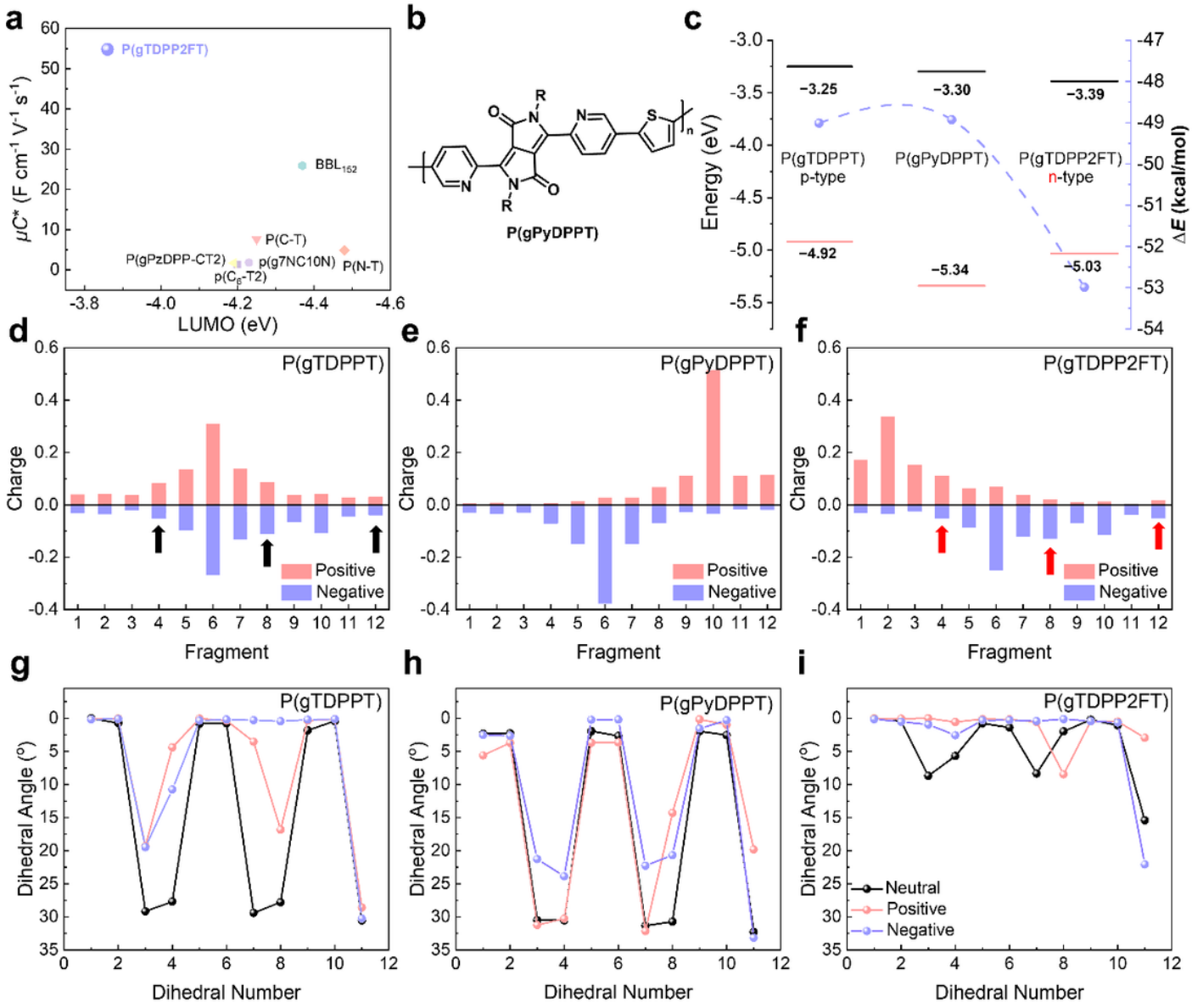

Figure 5

Understanding of the "doped state engineering". a Comparison of the LUMO energy levels measured by CV and μC^* of P(gTDPP2FT) and several reported n-type OECTs materials[25,27-30,38,42]. **b** Chemical structure of the reference polymer, P(gPyDPPT). **c** Comparison of the calculated HOMO/LUMO energy levels and the energy difference between neutral and negatively charged states ($\Delta E = E_{negative} - E_{neutral}$). Black lines stand for LUMO, and red lines stand for HOMO energy level. Purple dots stand for ΔE values. All the calculations are based on the trimers. **d-f** The charge distribution of the positively/negatively charged trimer for the three polymers. The charges of every fragment are the difference values between the charged state and the neutral state. The T and 2FT fragments of P(gTDPPT) and P(gTDPP2FT) are marked by black and red arrows, respectively. **g-i** The dihedral angle distribution between T/DPP/2FT/Py of the trimers in the neutral, positive, and negative states of the three polymers. The detailed fragment and dihedral numbers are shown in Fig. S9.

Supplementary Files

This is a list of supplementary files associated with this preprint. Click to download.

- PgTDPP2FTSI.pdf